SUPPLEMENTAL FIGURE AND MOVIE LEGENDS

FIGURE S1. Overall structural and assay information (related to Figure 2).
A, Representative electron density. $2|F_o|-|F_c|$ electron density is shown in gray contoured at 1σ over different portions of each RBX1-UBC12~NEDD8-CUL1^{CTD}-DCN1^{P} complex in the asymmetric unit (left and right panels). RBX1 is shown in blue, UBC12 in cyan, NEDD8 in yellow, CUL1 in green, and DCN1 in violet. Highlighted, from top to bottom are: RBX1 RING, linker, and W35 "pivot" interactions with NEDD8; DCN1^{P} interactions with UBC12's Acetyl Met and amino-terminal helix; CUL1 WHB subdomain, with neddylation site (Arg720 in structure) and stabilizing residue Tyr774 shown in stick representation; and the oxyester linkage between UBC12's C111S and NEDD8's C-terminal Gly76.

B, Crystallographic data and refinement statistics. Data for highest resolution shell is shown in parentheses. $R_{work} = \sum|F_o-F_c|/\sum|F_o|$. R_{free} is the cross-validation of R-factor, with 5% of the total reflections omitted in model refinement.

C, Comparable NEDD8 transfer from UBC12 to CUL1^{CTD}-RBX1 in pulse-chase assays, irrespective of version of NEDD8 and detection method. NEDD8 ligation assays either detected fluorescein-labeled NEDD8 or unlabeled NEDD8, depending on the quantity of NEDD8 required for a particular assay, expression of different NEDD8 variants, and availability of reagents when assays were conceptualized and/or performed. Left panel shows anti-NEDD8 immunoblot for time-course of pulse-chase assays monitoring transfer from UBC12 to CUL1^{CTD}-RBX1 for non-fluorescent and fluorescein-labeled NEDD8. Middle panel shows the same reaction for fluorescein-labeled NEDD8 detected for fluorescence using phosphorimager. Quantification (right) shows similar activity for both the fluorescein-labeled and unlabeled NEDD8, detected by immunoblotting or for fluorescence.

D, RBX1-UBC12~NEDD8-CUL1^{CTD}-DCN1^{P} complex structure reveals complementary UBC12-CUL1 interface.

Left: Close-up view of neddylation catalytic center, with CUL1's Lys720 modeled in red.

Right upper panel: Roles of UBC12 residues near interface with CUL1 in RBX1-dependent NEDD8 ligation. Pulse-chase assay monitoring time-course of RBX1-mediated fluorescent NEDD8 transfer to CUL1^{CTD} from the indicated UBC12 mutants located on the face contacting CUL1.

Right lower panel: Roles of CUL1 residues near interface with UBC12 in RBX1-dependent NEDD8 ligation. Pulse-chase assay monitoring time-course of RBX1-mediated fluorescent NEDD8 transfer from UBC12 to the indicated mutants of CUL1^{CTD} located on the face contacting UBC12.

FIGURE S2. Different roles for RBX1's canonical "linchpin" residue Asn98 toward different E2~UB intermediates (related to Figure 3).
A, Comparison of RING-E2~UBL assemblies, highlighting different contacts to canonical RING linchpin and the corresponding Asn98 from the neddylation complex. CBL RING-UBCH5B~UB (Dou et al., 2013) and RBX1 RING-UBC12~NEDD8 are shown superimposed over UB and NEDD8. Different roles for the canonical RING linchpin residues are exemplified by different contacts to their respective partner UBL's Gln40. The "canonical linchpin" (Arg412 from CBL) sidechain contacts UB's Gln40, which helps

guide the linchpin Arg into a crevice to coordinate UB and the E2 UBCH5. Through these interactions, UB's Gln40 and the canonical linchpin stabilize the active, closed conformation of the UBCH5~UB intermediate (Dou et al., 2012, 2013; Plechanovova et al., 2012; Pruneda et al., 2012). By contrast, NEDD8's Gln40 contacts the backbone nitrogen of RBX1's Asn98, which is located at the edge of the RBX1-UBC12~NEDD8 assembly. Thus, NEDD8's Gln40 interacts with the RBX1 RING domain, but does not play a central role in organizing the catalytically active conformation for the RBX1-UBC12~NEDD8 assembly, as the linchpin is shifted across the RING domain to RBX1's Arg46. These differences shed light on previous observations for the relative roles of UB's and NEDD8's Gln40 for ligation, identified through studies of Type III secretion system CHBP/Cif effectors from *Burkholderia pseudomallei* and enteropathogenic *Escherichia coli* (*EPEC)* (Crow et al., 2012; Cui et al., 2010; Yao et al., 2012). CHBP and Cif deamidate Gln40. In agreement with the structural differences for between RING-E2~UBL assemblies for UB and NEDD8, UB Gln40 deamidation was reported to almost eliminate UB transfer from UBCH5, whereas NEDD8 Gln40 deamidation was found to only slightly decrease NEDD8 transfer from UBC12 to a cullin (Cui et al., 2010; Toro et al., 2013).

B, Structure and models for RBX1 RING interactions with three distinct cognate E2~UBL intermediates, and roles of RBX1's Asn98 corresponding to the canonical RING linchpin defined in previous RING-UBCH5~UB structures (Dou et al., 2012, 2013; Plechanovova et al., 2012; Pruneda et al., 2012). RBX1 functions sequentially as a RING E3 with UBC12~NEDD8, UBCH5~UB, and CDC34~UB to modify distinct targets. First, RBX1 stimulates transfer of NEDD8 from UBC12 to a cullin, such as CUL1. Second, when the NEDD8~CUL1-RBX1 complex is assembled into an SCF and associated with an F-box protein, RBX1 can stimulate transfer of UB from UBCH5 to a ubiquitination target recruited to the F-box protein. Finally, RBX1 binds CDC34~UB, to promote UB transfer from CDC34 to the acceptor Lys48 on a UB-modified substrate bound to the F-box protein.

To compare interactions, RBX1 RING-UBC12~NEDD8 from the neddylation complex and the CBL RING-UBCH5B~UB assembly (Dou et al., 2013) were superimposed over NEDD8 and UB. CDC34 (Huang et al., 2014) was then superimposed on UBCH5B, based on prior mutational analysis consistent with the CDC34~UB closed conformation resembling that for UBCH5B~UB (Saha et al., 2011). The approximate location of a CDC34 acidic loop, disordered the crystal structure but potentially interacting with basic side-chains near the site of the canonical linchpin, is shown with dotted lines. These interactions would potentially be disfavored by a canonical linchpin Arg.

C, Role of canonical linchpin residue Asn98, tested through alanine and arginine substitutions, in RBX1 and UBCH5B-mediated ubiquitination of an SCF substrate. Time-course for pulse-chase ubiquitination assay monitoring transfer of fluorescent UB from UBCH5B to a Cyclin E phosphopeptide with the indicated versions of RBX1 in the context of neddylated $SCF^{FBW7\Delta D}$.

D, Assays testing role of Asn98, by substitution with alanine or a canonical linchpin Arg, in RBX1 and CDC34-mediated ubiquitination of an SCF substrate. Experiment was performed as in **C**, except with CDC34B and UB in which all lysines are substituted with arginines to prevent CDC34-dependent polyubiquitination.

E, Same as **D**, except monitoring transfer of wild-type UB from CDC34B.

FIGURE S3. RBX1-CUL1 conformational flexibility: function and regulation (related to Figure 4).

A, RBX1-CUL complexes display conformational flexibility (Duda et al., 2008), and functions of particular domain arrangements are beginning to emerge. The RBX1-UBC12~NEDD8-CUL1^{CTD}-DCN1^{P} structure described herein reveals the architecture for neddylation. Following NEDD8 ligation to a cullin, RBX1 promotes UB transfer from UBCH5 to a ubiquitination target. However, a model for a NEDD8~CUL1-RBX1 complex bound to UBCH5~UB based on the NEDD8 ligation complex and on prior RING-UBCH5~UB structures is consistent with further conformational changes, as follows. The model for the immediate product of the neddylation reaction is the RBX1-UBC12~NEDD8-CUL1^{CTD}-DCN1^{P} structure, except with NEDD8's covalent linkage transferred to CUL1, and with UBC12 released. To dock UBCH5B~UB on RBX1, the RING domains from RBX1 and CBL bound to UBCH5~UB (Dou et al., 2013) were superimposed. The model shows clashing between the donor UB and the NEDD8 ligated to CUL1, suggesting different RBX1-CUL1 conformation(s) are required for ubiquitination by a neddylated complex.

B, RBX1-CUL1 complexes display various conformations before, during, and after neddylation. Comparison of RBX1- CUL^{CTD} complexes reveals relative rotation of the RBX1 RING and cullin WHB domains. RBX1-UBC12~NEDD8-CUL1^{CTD}-DCN1^{P} structure is shown on the left in two views separated by 90° in y. To visualize different relative domain orientations, portions of various RBX1-CUL^{CTD} crystal structures are shown superimposed with the alpha/beta domain (RBX1 residues 22-34 and CUL1 residues 416-690) from the neddylation complex. The RBX1-CUL1-CAND1 complex (Goldenberg et al., 2004) represents a form prior to neddylation, which is inactive for UBL ligation. This RBX1-CUL^{CTD} architecture is commonly observed in crystal structures (Angers et al., 2006; Duda et al., 2008; Fischer et al., 2011; Goldenberg et al., 2004; Zheng et al., 2002). The two copies of RBX1-CUL5^{CTD}~NEDD8 complexes from the asymmetric unit (Duda et al., 2008) are shown on the right. These reveal potential for RBX1 RING and the neddylated CUL WHB domains to swing around post-neddylation.

C, Close-up showing rotation around the RBX1 Trp35 pivot in various structures. RBX1 is shown in ribbon diagram, with the Trp35 "pivot" and Ile37 "lever" side chains shown as sticks. The neddylation complex and other RBX1-CUL structures (Calabrese et al., 2011; Duda et al., 2008; Goldenberg et al., 2004) were aligned over the alpha/beta domain (RBX1 residues 22-34 and CUL1 residues 416-690), but for ease of viewing only RBX1 is shown.

D, Mass spectrometry identification of ubiquitination sites in reactions with "neddylized" donor UB (Q31E/D32E), UBCH5B, and NEDD8-modified SCF$^{FBW7\Delta D}$. Experiments were performed with three different instruments (Q-exactive, LTQ-Velos and Orbitrap Elite) and two different fragmentation methods (CID and HCD), which together reveal multiple modified sites on CUL1 (743 and 769 in the WHB subdomain), modification of NEDD8, and modification of UB. Although these data are not quantitative, nor do they necessarily identify all the ubiquitination sites, taken together with SDS-PAGE visualization of a ladder of at least five progressively slower migrating ubiquitinated NEDD8~CUL1 bands (Fig. 4J), the data are consistent with the neddylized UB being transferred to multiple sites, either on CUL1, NEDD8, or UB polyubiquitination. Given the requirement for the RBX1 lever for this reaction (Fig. 4K), the most likely explanation is that the RBX1 linker and RING and UBCH5~UB (Q31E, D32E) assemble into an active architecture as in the neddylation complex, and that multiple acceptor lysines can access the active site due to relative

rotation of at least a portion of the neddylated cullin (such as the WHB domain and its linked NEDD8) and the ligated UB.

FIGURE S4. Factors influencing reactivity of UBC12~NEDD8 intermediate (related to Figure 7).
A, Thioester-linked UBC12~NEDD8 discharges by ligation to CUL1 without substantial dissociation due to hydrolysis in the presence of the acceptor Lys720. Coomassie stained SDS-PAGE gels of time-course monitoring discharge of wild-type thioester-linked UBC12~NEDD8 intermediate in the presence of RBX1 in complex with wild-type (WT) CUL1, or CUL1 K720A mutant lacking the acceptor Lys. Reactions were performed at 30°C. Experiments in the presence of DTT show migration of products following reduction of the thioester-linked UBC12~NEDD8 intermediate. If not bound to RBX1-CUL1, the thioester-linked UBC12~NEDD8 intermediate can discharge via ligation by transferring NEDD8 to UBC12's lysine-rich N-terminal extension, resulting in an isopeptide-bonded, non-reducible UBC12~NEDD8 product (Huang et al., 2009).

B, Reactions performed as in **A**, except on ice.

C, CUL1 acceptor Lys720-dependent hydrolysis of an oxyester-linked UBC12~NEDD8 complex involves a known E2 catalytic element, the "catalytic Asn" (Wu et al., 2003). Coomassie stained SDS-PAGE gels of time-course monitoring discharge of the oxyester-linked UBC12 (N103S, C111S)~NEDD8 complex in the absence or presence of wild-type or indicated mutant variants of RBX1-CUL1^{CTD}, with or without DCN1^{P}, at 30°C. The N103S mutant slowed the reaction sufficiently to obtain a stable complex for crystallization.

D, The modeled CUL1 acceptor Lys720 contacts a loop that has potential to fluctuate based on differences amongst the UBC12 structures, and that is dynamic in other E2s (Berndsen et al., 2013; Dou et al., 2012; Yunus and Lima, 2006). Superposition of UBC12 from neddylation complex with a modeled CUL1 Lys720 acceptor, and previous structures of wild-type (1Y8X.pdb, blue) and C111A mutant (2NVU.pdb, light blue) versions of UBC12 (Huang et al., 2007; Huang et al., 2005).

D, Close-up view of modeled active site showing potential contacts to a UBC12~NEDD8 thioester bond and CUL1 acceptor Lys. The model contains reversions to wild-type sequences from the crystallographically trapped structures as follows: UBC12 Asn103 and Cys111, and CUL1 Lys720.

MOVIE S1. Overall structure of RBX1-UBC12~NEDD8-CUL1^{CTD}-DCN1^{P} Complex (related to Figure 2). Initially, the structure of RBX1-UBC12~NEDD8-CUL1^{CTD}-DCN1^{P} is shown in cartoon representation, with RBX1 in blue, UBC12 in cyan, NEDD8 in yellow, CUL1^{CTD} in green, and DCN1^{P} in violet. UBC12's active site C111S, its covalently-linked NEDD8 G76, the CUL1 acceptor site residue 720, and the zinc atoms from the RBX1 RING domain are shown in spheres. Juxtaposition between the UBC12~NEDD8 active site and the acceptor site from CUL1 is shown encircled. Next, the structure is rotated to highlight overall features of the E3s, including RBX's N-terminal strand recruiting CUL1, RBX1's RING binding to UBC12~NEDD8 in the activated closed conformation, and RBX1's linker connecting the N-terminal strand and C-terminal RING domain. DCN1-binding to UBC12's acetylated N-terminus is also shown. To give insight into the overall architecture, the structure is next represented in surface view and rotated, ultimately zooming in on the CUL1 acceptor in the UBC12~NEDD8 catalytic center.

MOVIE S2. NEDD8 directs its ligation machinery to CUL1 acceptor site (related to Figure 4). This movie shows comparison between the RBX1-UBC12~NEDD8-CUL1^{CTD}-DCN1^{P} structure and the prior, most common architecture for an RBX1 complex with a cullin CTD, represented here by coordinates from the RBX1-CUL1-CAND1 complex (Angers et al., 2006; Duda et al., 2008; Fischer et al., 2011; Goldenberg et al., 2004; Zheng et al., 2002). RBX1 is shown in blue, UBC12 in cyan, NEDD8 in yellow, CUL1^{CTD} in green, and DCN1^{P} in violet. First, the RBX1-UBC12~NEDD8-CUL1^{CTD}-DCN1^{P} structure is shown. Next, the RBX1 RING-UBC12~NEDD8 assembly in the conformation for neddylation was docked on the RBX1-CUL1^{CTD} portion of the prior RBX1-CUL1-CAND1 structure. This highlights the ~30 Å gap between the UBC12~NEDD8 active site and CUL1 acceptor Lys720 with RBX1 in this previously identified architecture. Rotation and zooming in shows clashing between the donor NEDD8, the RBX1 linker, and CUL1^{CTD} in the previously observed RBX1-CUL1 architecture. Thus, the previous architecture was compatible with CAND1 binding, but not neddylation. Note that the RBX1 "lever" and "pivot" would clash with NEDD8. Visualization of the RBX1 conformational change is aided by "morphing" between this inactive form and the catalytic RBX1-CUL1^{CTD} architecture for neddylation as revealed by the new structure. Some key residues establishing the neddylation architecture are RBX1 I37 "lever" and W35 "pivot", and NEDD8 Glu31 and Glu32.

EXTENDED EXPERIMENTAL PROCEDURES

Constructs, Protein Expression, and Purification

Expression constructs were prepared by standard molecular biology techniques and coding sequences entirely verified. Variations were introduced by PCR or QuikChange (Agilent). All protein sequences are human. Constructs and expression for many proteins and complexes have been described previously, as follows: APPBP1-UBA3 (NEDD8 E1), UBC12, and NEDD8 were described in (Huang and Schulman, 2005; Walden et al., 2003b); UBA1 (UB E1) and UBCH5B were described in (Huang et al., 2008; Kamadurai et al., 2013), UB, CDC34(B), and SKP1- FBW7ΔD (lacking the dimerization domain and corresponding to residues 263 to the C-terminus) were described in (Duda et al., 2012; Jubelin et al., 2010), CUL1-RBX1 (the "split 'n coexpress" version) was described in (Li et al., 2005; Zheng et al., 2002), CUL1^{CTD}-RBX1 (residues 411 to the C-terminus, with L421E, V451E, V452K, and Y455K mutations for improved solubility) and DCN1^{P} (residues 62 to the C-terminus) were described in (Huang et al., 2009; Scott et al., 2011). Neddylation and purification CUL1-RBX1 and variants was performed as described previously (Duda et al., 2008; Enchev et al., 2012). The crystallized UBC12 was expressed in insect cells for N-terminal acetylation, contained a Ser in place of the catalytic Cys111 and a Ser in place of Asn103 (the E2 asparagine promoting reactivity of E2~Ubl intermediates (Wu et al., 2003)), and harbored a His$_{6}$-tag fused to the C-terminus. This version of UBC12 was also used for experiments shown in Supplementary Fig. S4C. The version of UBC12 used in Fig. 7B-D was prepared similarly, except with a Ser substitution in place of the catalytic Cys111 and the wild-type Asn103. The version of UBCH5B used in Fig. 7E and F contained a Ser in place of the catalytic Cys85. CUL1^{CTD} K720A + Gly-Gly-Lys used in Fig. 1G contains the K720A mutation and the sequence Gly-Gly-Lys appended at the native C-terminus to place a lysine in spatial proximity to residue 720.

For experiments using oxyester-linked E2~UBL complexes, CUL1^{CTD}-RBX1, variants, and DCN1^{P} were purified as described (Calabrese et al., 2011; Scott et al., 2011), but with final gel filtration chromatography in using 25 mM HEPES, 200 mM NaCl, 1mM DTT, pH 7.5 to remove Tris buffers that contain primary amines. Oxyester-linked

UBC12~NEDD8 complexes were generated by mixing 60 μM UBC12 (N103S, C111S) or UBC12 (C111S), 4 μM APPBP1-UBA3, and 80 μM NEDD8 in 25 mM HEPES, 200 mM NaCl, 2.5 mM $MgCl_2$, 1 mM ATP, pH 7.5, and incubating at 30 °C for 18 hours. Oxyester-linked UBCH5B~UB complexes were generated by mixing 50 μM UBCH5B (C85S), 6 μM UBA1, 150 μM UB in 25 mM HEPES, 200 mM NaCl, 2.5 mM $MgCl_2$, 1 mM ATP, pH 7.5. After diluting the reaction mixtures into 25 mM MES, 20 mM NaCl, 1 mM DTT, pH 6.5, the oxyester-linked E2~UBL complexes were purified by ion exchange chromatography using a Resource-S column, and gel filtration chromatography in 25 mM HEPES, 200 mM NaCl, pH 7.5.

To label NEDD8, UB, and variants with a fluorescent tag, a cysteine was introduced into pGEX-2TK-NEDD8 and pGEX-2TK-UB constructs (Duda et al., 2008; Walden et al., 2003b) by replacing the N-terminal RRASV site for Protein Kinase A with RRACV. 10 mM DTT was added to the purified NEDD8, UB and variants, followed by a 30-minute incubation on ice to ensure complete reduction of the single cysteine for labeling. Proteins were then buffer exchanged over NAP-5 columns (GE Healthcare) into labeling buffer (25 mM HEPES, 200 mM NaCl, pH7.5). Protein concentrations were determined based on absorption at 280 nm (NanoDrop) with extinction coefficients calculated by the ExPASy server, and diluted to a final concentration of 220 μM in labeling buffer. Fluorescein-5-maleimide (Life Technologies) was added to a final concentration of 1 mM and mixtures incubated at room temperature for 2 hours. The reaction mixture was passed over a NAP-5 column to remove residual free dye, and the eluate was concentrated and further purified by gel filtration using a Superdex SD-75 gel column (GE) to remove free, unreacted dye. Labeling efficiently was determined by measuring the ratio of protein concentration to fluorescein concentration measured at 495 nm. In all cases the labeling efficiency was measured at ≥ 80%.

X-ray Crystallography

Crystals were grown at 4 °C, by the hanging-drop vapor-diffusion method. Crystals were obtained from a mixture of the oxyester-linked UBC12 (N-terminally acetylated, N103S, C111S)~NEDD8 complex, RBX1- $CUL1^{CTD}$ (K720R), and $DCN1^{P}$ at a ratio of 40 μM: 35 μM: 40 μM, respectively, with a morphology resembling tiny sea urchins/clusters of needles and plates in 18-22% PEG3350, 0.2M Ammonium Citrate, pH 7.0. Single, diffraction quality crystals were obtained by microseeding into drops containing approximate five-fold concentrated protein complex mixture (160 μM: 150 μM: 160 μM UBC12 (N-terminally acetylated, N103S, C111S)~NEDD8 : RBX1- $CUL1^{CTD}$ (K720R): $DCN1^{P}$) in 11% PEG3350, 0.2 M Ammonium Citrate 10 mM ATP, pH 6.7. Despite these improvements, and exhaustive unsuccessful additional attempts to improve quality, the crystals grew as thin plates resembling sheets of paper. Among the approaches we tried in attempts to improve crystals was use of selenomethionine-labeled proteins, with the hope that selenomethionine could enhance crystal packing. Although this approach did not improve the crystals, anomalous datasets for isomorphous crystals grown with selenomethionine-labeled $DCN1^{P}$, NEDD8, and NEDD8 (L62SeM) provided unbiased validation of the structure through localization of selenium atoms.

Crystals were harvested by soaking for 1-5 minutes with crystallization solution supplemented with 12% and 24% ethylene glycol in sequential steps, prior to flash-freezing in liquid nitrogen. Reflection data were collected at NECAT ID-24-E at the Advanced Photon Source. The crystals belong to space group $P2_1$. The two copies of the RBX1-UBC12~NEDD8-$CUL1^{CTD}$-$DCN1^{P}$ complex in the asymmetric unit superimpose with 0.395 Å RMSD as measured by COOT SSM Superpose, so only one is discussed in the main text. Reflection data were processed with HKL2000 (Otwinowski and Minor,

1997). Phases were obtained by molecular replacement using PHASER (McCoy et al., 2007) using the following search models: (1) 2 copies of RBX1^{NTD} (residues 19-33)-CUL1^{CTD} (residues 411-705) lacking the WHB subdomain from 1LDK.pdb (Zheng et al., 2002) (2) 2 copies of CUL1^{WHB} (residues 710-776)-DCN1^{P} (residues 62-253) from 3TDZ.pdb (Scott et al., 2011) and (3) 2 copies of UBC12 (residues 27-183) from 1Y8X.pdb (Huang et al., 2005). The RBX1 RING domain (residues 41-105) (Goldenberg et al., 2004) was subsequently placed manually utilizing an anomalous map as a guide for locations of the three zinc coordination sites per RING domain. UBC12's acetylated amino-terminus was built manually. Ultimately, NEDD8 (Whitby et al., 1998) and the RBX1 linker sequence were manually fitted into their respective electron density. Manual rebuilding was performed with COOT (Emsley et al., 2010) and Refinement was performed using Phenix (Adams et al., 2010). Electron density is high quality with the exception of some CUL1^{CTD} loops that are most distal from the neddylation active site, not stabilized by crystal packing, and which are often not visible in CUL structures. The final model contains CUL1 residues 416-612, 620-648, 665-669, and 681-776 (Chain A), 416-596, 600-610, 620-649, 665-669, 682-776 (Chain C); RBX1 residues 23-59 and 67-104 (Chain B), 23-59 and 67-105 (Chain D); DCN1 residues 62-258 (Chain E), 64-258 (Chain F), UBC12 with N-terminal acetylation and residues 1-15 and 29-184 (Chain G), 1-13 and 29-184 (Chain I); and NEDD8 residues 1-76 (Chains H and K). Details of Refinement are provided in Supplementary Figure S1B.

Structure analysis was performed using COOT (Emsley et al., 2010) and Pymol (http://pymol.sourceforge.net), and the morphing was performed using Chimera (Pettersen et al., 2004). Figures were made with Pymol, and structure superimposition was performed with the "Align" function.

Biochemical Assays

UBL modification of CUL1 was monitored using pulse-chase assays to exclusively monitor the effects of mutations on ligation to CUL1, without sensing other reactions involved in UBL transfer. For the "pulse" reaction, thioester-linked E2~UBL intermediates were generated by incubating 10 μM UBC12 or UBCH5B, 15 μM NEDD8, UB, or variants (unlabeled or fluorescein-labeled as indicated), and 400 nM APPBP1-UBA3 or UBA1 in 25 mM HEPES, 200 mM NaCl, 2.5 mM $MgCl_2$, 1 mM ATP, pH 7.5 for 15 minutes at room temperature. The pulse formation of thioester-linked E2~UBL intermediates was quenched with 50 mM EDTA on ice for 5 minutes. For the "chase", UBL transfer from E2 to target was performed by diluting the E2~UBL thioester conjugate to 0.4 μM in 50 mM Tris, 50 mM NaCl, 50 mM EDTA, 0.5 mg/ml BSA, pH 6.8 on ice, and adding RBX1-CUL1^{CTD} or mutant variants at a final concentration of 0.8 μM. Reactions in Figures 1, 3-5 and S1 monitor RBX1-dependent UBL transfer, in the absence of DCN1^{P}. Aliquots were removed at the indicated times and terminated with 2X SDS-PAGE sample buffer. Reaction products were separated on 4-12% NuPAGE gels (Invitrogen). Fluorescent gels were visualized by scanning on a Typhoon imager (GE).

For bar graphs shown in Figures 1, 4, and 5, gel bands were quantified from fluorescent scans using ImageQuant (GE) software associated with the imager, and from Western Blots using ImageJ (NIH). The amount of UBL~CUL1^{CTD} formed at each time-point was standardized to the amount of E2~UBL at the start of the reaction. Rates were then calculated by fitting the curves for UBL transfer over time to a non-linear quadratic equation (second-order polynomial) using Prism. Each series was normalized by dividing the rate for each variant by that of WT, such within a given panel, wild-type RBX1-CUL1, E2, and UBL have a normalized rate of 1 for the ligation reaction. Errors represent +/- one standard deviation for the rate prior to normalization. Experiments were performed 3-4 times.

To make non-cognate E2~UBL intermediates used in Fig. 1D, 1E, 6F, and 6G, we took advantage of altered specificity mutant versions of NEDD8's E1, NEDD8, or UB that bypass the gating that prevents misactivation of UB by NEDD8's E1 and vice-versa (Bohnsack and Haas, 2003; Souphron et al., 2008; Walden et al., 2003a; Whitby et al., 1998). Briefly, residue 72, an alanine in NEDD8 and an arginine in UB, determines ability to bind to and be activated by NEDD8's or UB's E1, and therefore to be loaded onto an E2 catalytic cysteine. UBC12~UB was generated with an R190Q mutant version of the UBA3 subunit of NEDD8's E1, which compensates for UB's Arg72 that normally restricts access to NEDD8's E1. Swapping the identity of residue 72 between NEDD8 and UB also swaps E1 specificity, thus enabling use of APPBP1-UBA3 (NEDD8's E1) to make the thioester-linked UBC12~UB R72A intermediate and of UBA1 (UB's E1) to make the thioester-linked UBCH5B~NEDD8 A72R intermediate.

Transfer of NEDD8 to CUL1 in the presence of DCN1^{P} is swift, and for Fig. 6E and F, in order to visualize a linear progression of product formation we employed the use of a KinTeK RGF-3 quench flow instrument. Briefly, generation and quenching of the thioester-linked conjugate was performed as described above. Chase reactions were carried out as described above, except in the absence or presence of 10 μM DCN1^{P} and at 20 °C. Reactions were terminated with 2X SDS-PAGE sample buffer at the indicated times, and products were separated and visualized as described above.

For pulse-chase assays monitoring neddylated SCF$^{FBW7\Delta D}$-dependent ubiquitination of a Cyclin E phosphopeptide (Duda et al., 2012) in Fig. 4J, K, and Fig. S2C-E, thioester-linked UBCH5B~UBL intermediates were generated and quenched as described above. 30 minutes prior to initiation of the chase reactions, SCF complexes were equilibrated on ice by mixing the components to a final concentration of 1 μM RBX1-CUL1, 1 μM SKP1-FBW7ΔD, and 5 μM Cyclin E phosphopeptide in 50mM HEPES, 20 mM NaCl, pH 7.5. Chase reactions were performed at room temperature, and involved diluting the thioester-linked UBCH5B~UBL intermediate to 0.3 μM in 50 mM HEPES, 20 mM NaCl, 50 mM EDTA, 0.5 mg/ml BSA, pH7.5 and addition of the SCF complex mixture to a final concentration of 0.4 μM. Aliquots were removed at the indicated times and quenched with 2X SDS-PAGE sample buffer. Reaction products were separated and visualized as described above.

We initially monitored the stability of various oxyester-linked versions of UBC12 (C111S)~NEDD8, mixed with various components of the neddylation machinery, to identify complexes sufficiently stable for X-ray crystallography, and then adapted the protocol to examine discharge via ligation versus hydrolysis in Figures 7 and S4. Various versions of oxyester-linked UBC12 (C111S)~NEDD8 complexes were mixed at 30°C at a final concentration of 25 μM with buffer, or mixtures that contained 25 μM WT CUL1^{CTD}-RBX1 or mutant variants in the presence or absence of 25 μM DCN1^{P} that had been equilibrated at 30 °C for 5 minutes. Experiments were performed in 25 mM HEPES, 50 mM NaCl, pH 7.5. An aliquot was removed immediately to represent the zero minute time-point and additional aliquots removed at the indicated times and quenched with 2X SDS-PAGE sample buffer. Reactions products were separated on 4-12% NuPAGE gels and visualized by staining with Coomassie blue.

We modified our standard pulse-chase assay in an attempt to determine if the thioester-linked UBC12~NEDD8 intermediate would hydrolyze to a significant extent, as observed for the oxyester conjugate, when exposed to wild-type RBX1-CUL1^{CTD}. In order to accomplish this it was imperative to modify the "pulse" reaction to effectively convert the entire pool of NEDD8 to a thioester-linked conjugate with UBC12. This allowed visualization of the product of hydrolysis by the appearance of free NEDD8. The modified "pulse" reaction consisted of 100 μM Ubc12, 2 μM APPBP1-UBA3, and 80 μM NEDD8 in

25 mM HEPES, 100 mM NaCl, 2.5 mM $MgCl_2$, 1 mM ATP, pH 7.5. This pulse loading reaction was incubated at room temperature for 20 minutes and quenched by the addition of 50 mU Apyrase (New England Biolabs) to hydrolyze free ATP. Prior to the chase, a mock solution containing buffer, or reaction components of 25 μM wild-type or mutant versions of RBX1-$CUL1^{CTD}$ with or without 25 μM $DCN1^{P}$, were equilibrated at 30°C for 5 minutes. Chase reactions were initiated by the addition of the thioester-linked UBC12~NEDD8 intermediate to 25 μM. Aliquots were removed and processed as described for the assays for stability and reactivity of oxyester-linked E2~UBL conjugates. Reaction products were visualized by Coomassie blue staining.

Mass spectrometry

Peptides generated from Trypsin or sequential Trypsin/LysC digestion of reaction as in Fig. 4J and K (with UBCH5B~UB Q31E/D32E (i.e. neddylized), NEDD8~CUL1-RBX1, FBW7ΔD and Cyclin E phosphopeptide) was desalted offline using C18 stage tips. Peptides were eluted from the stage tip, dried down using a speed vac, and resuspended in 10 μl 5% formic acid, 5% acetonitrile. MS/MS data was generated using an LTQ-Velos mass spectrometer (Thermo Fisher Scientific, Waltham, MA, USA), resultant MS/MS spectra were searched with Sequest prior to target-decoy peptide filtering and linear discriminant analysis to control the peptide level false-positive rate (Huttlin et al., 2010). The same peptide mixture was subsequently analyzed on either a Q-Exactive Mass Spectrometer (Thermo Fisher Scientific, Waltham, MA, USA) or Orbitrap Elite Mass Spectrometer (Thermo Fisher Scientific, Waltham, MA, USA) and resultant MS/MS spectra were analyzed as indicated previously (Kim et al., 2011).

SUPPLEMENTAL REFERENCES

Adams, P.D., Afonine, P.V., Bunkoczi, G., Chen, V.B., Davis, I.W., Echols, N., Headd, J.J., Hung, L.W., Kapral, G.J., Grosse-Kunstleve, R.W., *et al.* (2010). PHENIX: a comprehensive Python-based system for macromolecular structure solution. Acta crystallographica *66*, 213-221.

Angers, S., Li, T., Yi, X., MacCoss, M.J., Moon, R.T., and Zheng, N. (2006). Molecular architecture and assembly of the DDB1-CUL4A ubiquitin ligase machinery. Nature *443*, 590-593.

Berndsen, C.E., Wiener, R., Yu, I.W., Ringel, A.E., and Wolberger, C. (2013). A conserved asparagine has a structural role in ubiquitin-conjugating enzymes. Nat Chem Biol *9*, 154-156.

Bohnsack, R.N., and Haas, A.L. (2003). Conservation in the mechanism of Nedd8 activation by the human AppBp1-Uba3 heterodimer. The Journal of biological chemistry *278*, 26823-26830.

Calabrese, M.F., Scott, D.C., Duda, D.M., Grace, C.R., Kurinov, I., Kriwacki, R.W., and Schulman, B.A. (2011). A RING E3-substrate complex poised for ubiquitin-like protein transfer: structural insights into cullin-RING ligases. Nature structural & molecular biology *18*, 947-949.

Crow, A., Hughes, R.K., Taieb, F., Oswald, E., and Banfield, M.J. (2012). The molecular basis of ubiquitin-like protein NEDD8 deamidation by the bacterial effector protein Cif. Proceedings of the National Academy of Sciences of the United States of America *109*, E1830-1838.

Cui, J., Yao, Q., Li, S., Ding, X., Lu, Q., Mao, H., Liu, L., Zheng, N., Chen, S., and Shao, F. (2010). Glutamine deamidation and dysfunction of ubiquitin/NEDD8 induced by a bacterial effector family. Science (New York, NY *329*, 1215-1218.

Dou, H., Buetow, L., Sibbet, G.J., Cameron, K., and Huang, D.T. (2012). BIRC7-E2 ubiquitin conjugate structure reveals the mechanism of ubiquitin transfer by a RING dimer. Nature structural & molecular biology *19*, 876-883.

Dou, H., Buetow, L., Sibbet, G.J., Cameron, K., and Huang, D.T. (2013). Essentiality of a non-RING element in priming donor ubiquitin for catalysis by a monomeric E3. Nature structural & molecular biology *20*, 982-986.

Duda, D.M., Borg, L.A., Scott, D.C., Hunt, H.W., Hammel, M., and Schulman, B.A. (2008). Structural insights into NEDD8 activation of cullin-RING ligases: conformational control of conjugation. Cell *134*, 995-1006.

Duda, D.M., Olszewski, J.L., Tron, A.E., Hammel, M., Lambert, L.J., Waddell, M.B., Mittag, T., DeCaprio, J.A., and Schulman, B.A. (2012). Structure of a glomulin-RBX1-CUL1 complex: inhibition of a RING E3 ligase through masking of its E2-binding surface. Molecular cell *47*, 371-382.

Emsley, P., Lohkamp, B., Scott, W.G., and Cowtan, K. (2010). Features and development of Coot. Acta crystallographica *66*, 486-501.

Enchev, R.I., Scott, D.C., da Fonseca, P.C., Schreiber, A., Monda, J.K., Schulman, B.A., Peter, M., and Morris, E.P. (2012). Structural basis for a reciprocal regulation between SCF and CSN. Cell reports *2*, 616-627.

Fischer, E.S., Scrima, A., Bohm, K., Matsumoto, S., Lingaraju, G.M., Faty, M., Yasuda, T., Cavadini, S., Wakasugi, M., Hanaoka, F.*, et al.* (2011). The molecular basis of CRL4DDB2/CSA ubiquitin ligase architecture, targeting, and activation. Cell *147*, 1024-1039.

Goldenberg, S.J., Cascio, T.C., Shumway, S.D., Garbutt, K.C., Liu, J., Xiong, Y., and Zheng, N. (2004). Structure of the Cand1-Cul1-Roc1 complex reveals regulatory mechanisms for the assembly of the multisubunit cullin-dependent ubiquitin ligases. Cell *119*, 517-528.

Huang, D.T., Ayrault, O., Hunt, H.W., Taherbhoy, A.M., Duda, D.M., Scott, D.C., Borg, L.A., Neale, G., Murray, P.J., Roussel, M.F.*, et al.* (2009). E2-RING expansion of the NEDD8 cascade confers specificity to cullin modification. Molecular cell *33*, 483-495.

Huang, D.T., Hunt, H.W., Zhuang, M., Ohi, M.D., Holton, J.M., and Schulman, B.A. (2007). Basis for a ubiquitin-like protein thioester switch toggling E1-E2 affinity. Nature *445*, 394-398.

Huang, D.T., Paydar, A., Zhuang, M., Waddell, M.B., Holton, J.M., and Schulman, B.A. (2005). Structural basis for recruitment of Ubc12 by an E2 binding domain in NEDD8's E1. Molecular cell *17*, 341-350.

Huang, D.T., and Schulman, B.A. (2005). Expression, purification, and characterization of the E1 for human NEDD8, the heterodimeric APPBP1-UBA3 complex. Methods in enzymology *398*, 9-20.

Huang, D.T., Zhuang, M., Ayrault, O., and Schulman, B.A. (2008). Identification of conjugation specificity determinants unmasks vestigial preference for ubiquitin within the NEDD8 E2. Nature structural & molecular biology *15*, 280-287.

Huang, H., Ceccarelli, D.F., Orlicky, S., St-Cyr, D.J., Ziemba, A., Garg, P., Plamondon, S., Auer, M., Sidhu, S., Marinier, A.*, et al.* (2014). E2 enzyme inhibition by stabilization of a low-affinity interface with ubiquitin. Nat Chem Biol *10*, 156-163.

Huttlin, E.L., Jedrychowski, M.P., Elias, J.E., Goswami, T., Rad, R., Beausoleil, S.A., Villen, J., Haas, W., Sowa, M.E., and Gygi, S.P. (2010). A tissue-specific atlas of mouse protein phosphorylation and expression. Cell *143*, 1174-1189.

Jubelin, G., Taieb, F., Duda, D.M., Hsu, Y., Samba-Louaka, A., Nobe, R., Penary, M., Watrin, C., Nougayrede, J.P., Schulman, B.A.*, et al.* (2010). Pathogenic bacteria target NEDD8-conjugated cullins to hijack host-cell signaling pathways. PLoS Pathog *6*.

Kamadurai, H.B., Qiu, Y., Deng, A., Harrison, J.S., Macdonald, C., Actis, M., Rodgrigues, P., Miller, D.J., Souphron, J., Lewis, S.M., *et al.* (2013). Mechanism of ubiquitin ligation and lysine prioritization by a HECT E3. eLIFE.

Kim, W., Bennett, E.J., Huttlin, E.L., Guo, A., Li, J., Possemato, A., Sowa, M.E., Rad, R., Rush, J., Comb, M.J., *et al.* (2011). Systematic and quantitative assessment of the ubiquitin-modified proteome. Molecular cell *44*, 325-340.

Li, T., Pavletich, N.P., Schulman, B.A., and Zheng, N. (2005). High-level expression and purification of recombinant SCF ubiquitin ligases. Methods in enzymology *398*, 125-142.

McCoy, A.J., Grosse-Kunstleve, R.W., Adams, P.D., Winn, M.D., Storoni, L.C., and Read, R.J. (2007). Phaser crystallographic software. J Appl Crystallogr *40*, 658-674.

Otwinowski, Z., and Minor, W. (1997). Processing of X-ray Diffraction Data Collected in Oscillation Mode. Methods in Enzymology, Macromolecular Crystallography, part A *276*, 307-326.

Pettersen, E.F., Goddard, T.D., Huang, C.C., Couch, G.S., Greenblatt, D.M., Meng, E.C., and Ferrin, T.E. (2004). UCSF Chimera--a visualization system for exploratory research and analysis. J Comput Chem *25*, 1605-1612.

Plechanovova, A., Jaffray, E.G., Tatham, M.H., Naismith, J.H., and Hay, R.T. (2012). Structure of a RING E3 ligase and ubiquitin-loaded E2 primed for catalysis. Nature *489*, 115-120.

Pruneda, J.N., Littlefield, P.J., Soss, S.E., Nordquist, K.A., Chazin, W.J., Brzovic, P.S., and Klevit, R.E. (2012). Structure of an E3:E2 approximately Ub Complex Reveals an Allosteric Mechanism Shared among RING/U-box Ligases. Molecular cell *47*, 933-942.

Saha, A., Lewis, S., Kleiger, G., Kuhlman, B., and Deshaies, R.J. (2011). Essential role for ubiquitin-ubiquitin-conjugating enzyme interaction in ubiquitin discharge from Cdc34 to substrate. Molecular cell *42*, 75-83.

Scott, D.C., Monda, J.K., Bennett, E.J., Harper, J.W., and Schulman, B.A. (2011). N-terminal acetylation acts as an avidity enhancer within an interconnected multiprotein complex. Science (New York, NY *334*, 674-678.

Souphron, J., Waddell, M.B., Paydar, A., Tokgoz-Gromley, Z., Roussel, M.F., and Schulman, B.A. (2008). Structural dissection of a gating mechanism preventing misactivation of ubiquitin by NEDD8's E1. Biochemistry *47*, 8961-8969.

Toro, T.B., Toth, J.I., and Petroski, M.D. (2013). The cyclomodulin cycle inhibiting factor (CIF) alters cullin neddylation dynamics. The Journal of biological chemistry *288*, 14716-14726.

Walden, H., Podgorski, M.S., Huang, D.T., Miller, D.W., Howard, R.J., Minor, D.L., Jr., Holton, J.M., and Schulman, B.A. (2003a). The structure of the APPBP1-UBA3-NEDD8-ATP complex reveals the basis for selective ubiquitin-like protein activation by an E1. Molecular cell *12*, 1427-1437.

Walden, H., Podgorski, M.S., and Schulman, B.A. (2003b). Insights into the ubiquitin transfer cascade from the structure of the activating enzyme for NEDD8. Nature *422*, 330-334.

Whitby, F.G., Xia, G., Pickart, C.M., and Hill, C.P. (1998). Crystal structure of the human ubiquitin-like protein NEDD8 and interactions with ubiquitin pathway enzymes. The Journal of biological chemistry *273*, 34983-34991.

Wu, P.Y., Hanlon, M., Eddins, M., Tsui, C., Rogers, R.S., Jensen, J.P., Matunis, M.J., Weisman, A.M., Wolberger, C., and Pickart, C.M. (2003). A conserved catalytic residue in the ubiquitin-conjugating enzyme family. The EMBO journal *22*, 5241-5250.

Yao, Q., Cui, J., Wang, J., Li, T., Wan, X., Luo, T., Gong, Y.N., Xu, Y., Huang, N., and Shao, F. (2012). Structural mechanism of ubiquitin and NEDD8 deamidation catalyzed by bacterial effectors that induce macrophage-specific apoptosis. Proceedings of the National Academy of Sciences of the United States of America *109*, 20395-20400.

Yunus, A.A., and Lima, C.D. (2006). Lysine activation and functional analysis of E2-mediated conjugation in the SUMO pathway. Nature structural & molecular biology *13*, 491-499.

Zheng, N., Schulman, B.A., Song, L., Miller, J.J., Jeffrey, P.D., Wang, P., Chu, C., Koepp, D.M., Elledge, S.J., Pagano, M., *et al.* (2002). Structure of the Cul1-Rbx1-Skp1-F boxSkp2 SCF ubiquitin ligase complex. Nature *416*, 703-709.

Supplemental Figure 1

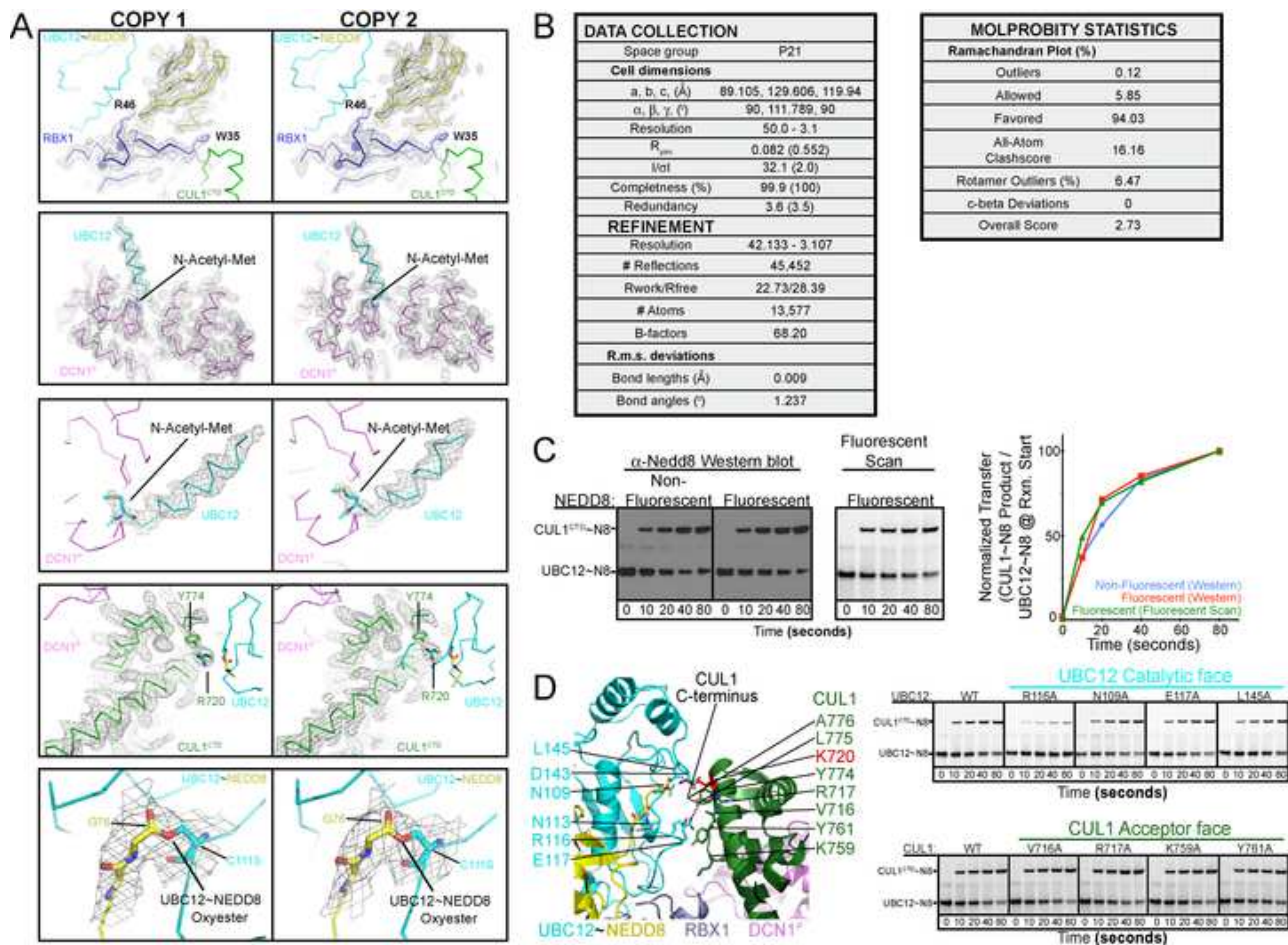

DATA COLLECTION	
Space group	P21
Cell dimensions	
a, b, c, (Å)	89.105, 129.606, 119.94
α, β, γ, (°)	90, 111.789, 90
Resolution	50.0 - 3.1
R_{pim}	0.082 (0.552)
I/σI	32.1 (2.0)
Completeness (%)	99.9 (100)
Redundancy	3.6 (3.5)
REFINEMENT	
Resolution	42.133 - 3.107
# Reflections	45,452
Rwork/Rfree	22.73/28.39
# Atoms	13,577
B-factors	68.20
R.m.s. deviations	
Bond lengths (Å)	0.009
Bond angles (°)	1.237

MOLPROBITY STATISTICS	
Ramachandran Plot (%)	
Outliers	0.12
Allowed	5.85
Favored	94.03
All-Atom Clashscore	16.16
Rotamer Outliers (%)	6.47
c-beta Deviations	0
Overall Score	2.73

Supplemental Figure 2

A

R72
Q40
G35
G35
Q40
R412
Q92
H77
H390
N98
UBC12~NEDD8
UBCH5B~UB
RBX1 RING
CBL RING

B

UBC12~NEDD8
UBCH5B~UB
CDC34
K720 Model
CUL1^{CTD}
RBX1 RING
CBL RING
CDC34's Acidic Loop
CBL "Linchpin" Arginine
RBX1 N98

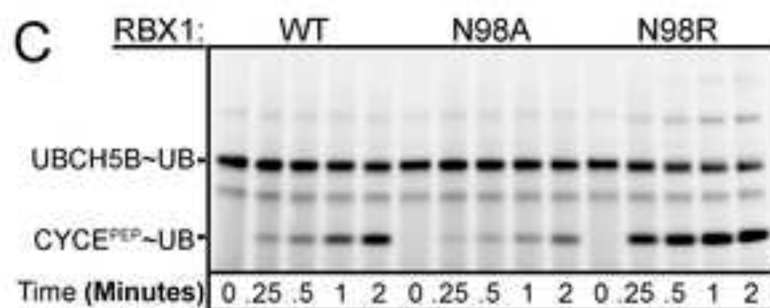

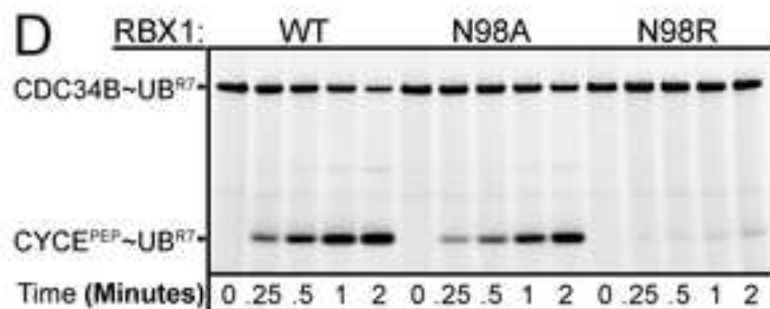

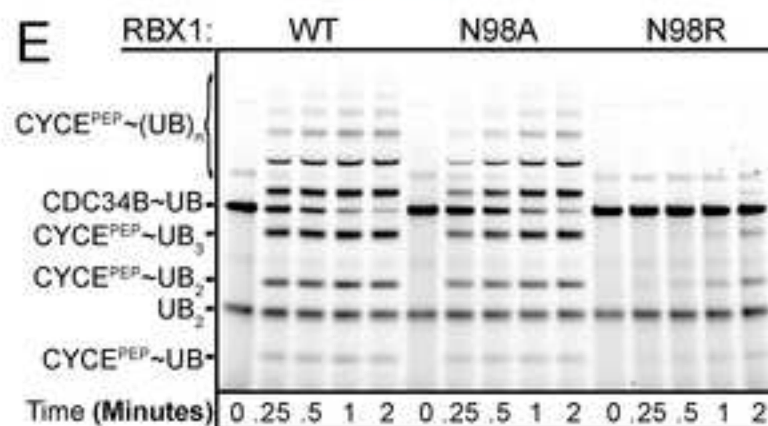

Supplemental Figure 3

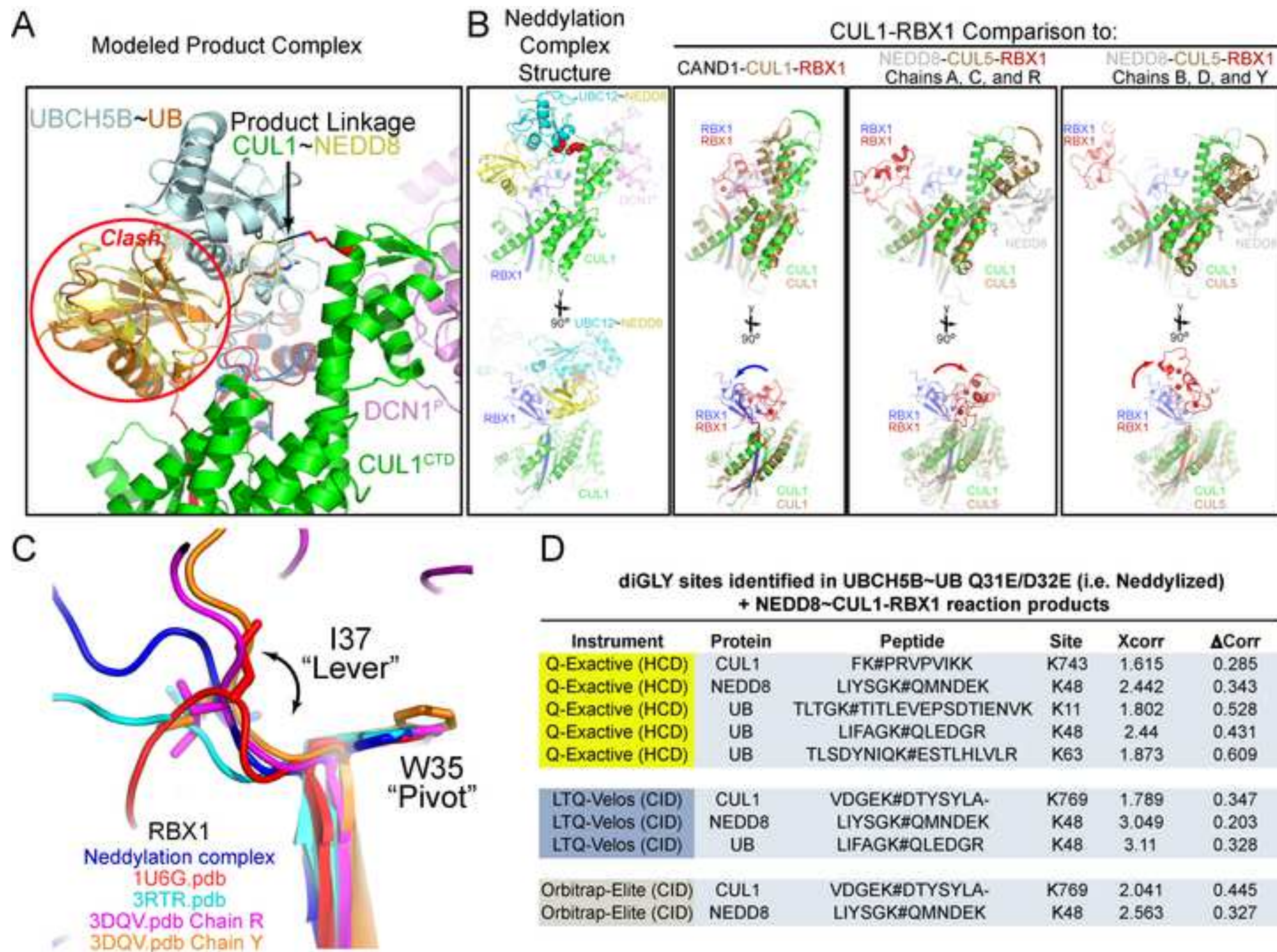

diGLY sites identified in UBCH5B~UB Q31E/D32E (i.e. Neddylized) + NEDD8~CUL1-RBX1 reaction products

Instrument	Protein	Peptide	Site	Xcorr	ΔCorr
Q-Exactive (HCD)	CUL1	FK#PRVPVIKK	K743	1.615	0.285
Q-Exactive (HCD)	NEDD8	LIYSGK#QMNDEK	K48	2.442	0.343
Q-Exactive (HCD)	UB	TLTGK#TITLEVEPSDTIENVK	K11	1.802	0.528
Q-Exactive (HCD)	UB	LIFAGK#QLEDGR	K48	2.44	0.431
Q-Exactive (HCD)	UB	TLSDYNIQK#ESTLHLVLR	K63	1.873	0.609
LTQ-Velos (CID)	CUL1	VDGEK#DTYSYLA-	K769	1.789	0.347
LTQ-Velos (CID)	NEDD8	LIYSGK#QMNDEK	K48	3.049	0.203
LTQ-Velos (CID)	UB	LIFAGK#QLEDGR	K48	3.11	0.328
Orbitrap-Elite (CID)	CUL1	VDGEK#DTYSYLA-	K769	2.041	0.445
Orbitrap-Elite (CID)	NEDD8	LIYSGK#QMNDEK	K48	2.563	0.327

Supplemental Figure 4

Click here to download high resolution image